Inorganic Chemistry

ARTICLE

pubs.acs.org/IC

Chiral Semiconductor Phases: The Optically Pure $D_3[M^{III}(S,S\text{-EDDS})]_2$ (D = TTF, TSF) Family

Nikola Paul Chmel,[†] Guy J. Clarkson,[†] Alessandro Troisi,[†] Scott S. Turner,[‡] and Peter Scott*[,†]

[†]Department of Chemistry, University of Warwick, Gibbet Hill Road, Coventry, CV4 7AL, United Kingdom

[‡]Department of Chemistry, University of Surrey, Guildford, Surrey, GU2 7XH, United Kingdom

Supporting Information

ABSTRACT: A new family of optically pure tetrathiafulvalenium and tetraselenafulvalenium salts, $D_3[M^{III}(S,S\text{-EDDS})]_2 \cdot nH_2O$ (where D = TTF, TSF; M = Co, Fe, Cr; EDDS = ethylenediaminedisuccinato), were synthesized electrochemically. These phases are semiconductors with conductivities between 6.9×10^{-6} and 1.3×10^{-5} S·cm^{-1} (E_a *ca.* 0.3 eV) for TTF and 2.8×10^{-4} to 2.8×10^{-5} S·cm^{-1} (E_a *ca.* 0.1 eV) for TSF compounds. While some crystals suffer from twinning, other well resolved structures consist of TTF/TSF stacks which, under the influence of the chiral anion, exhibit a periodic undulation described by an elliptical helix. The crystallographic data, along with computational work, indicate charge localization in the semiconducting motifs.

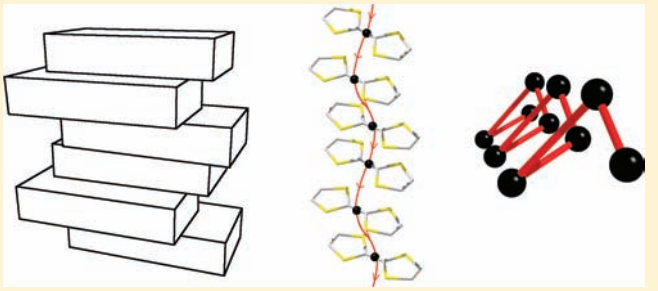

INTRODUCTION

The recent discovery of magnetic chiral anisotropy (MCA) has ignited interest in chiral conductors, since the resistance of such materials is expected to depend on the external magnetic field, the current, and the handedness of the medium.[1,2] This gives rise to the possibility of applications in spintronics-based devices or as magneto chiral switches.[1,3] Hitherto, the presence of the effect was demonstrated only in two cases.[1,4] Different approaches toward this problem include the use of chiral carbon nanotubes,[2,4] helical polymers,[5] supramolecular nanocoils,[6] and charge-transfer materials based on tetrathiafulvalene (TTF) and its derivatives.[7−11]

In respect to the latter, relatively few systems are chiral and optically pure.[12] Chirality may be introduced into the structure of the donor molecule or *via* a chiral auxiliary, *i.e.*, solvent, counterion, or guest molecule.[7,8,10,13−15] Our efforts in this field have focused on the synthesis of charge transfer salts of *achiral* organic donor species such as TTF and the selenium analogue TSF with optically pure anions.[16] The hypothesis behind our use of this approach was that if the chirality is too well expressed in the conducting phase (*i.e.*, is substantially twisted or otherwise asymmetric), then low conductivity is the likely outcome. The difficulty with this approach however is that few optically pure anions are available in a suitable form.

Complexes of a chiral hexadentate chelating agent, ethylenediaminedisuccinic acid (H_4EDDS)[17,18] (Figure 1), have recently aroused our interest due to their ready availability as optically pure samples; complexes of homochiral EDDS form one diastereoisomer exclusively. Unfortunately, these compounds show very poor solubility in nonaqueous solvents. Recently, we have developed synthetic routes toward the first readily available, organic soluble family of EDDS complexes, $PPh_4[M^{III}(S,S\text{-EDDS})] \cdot 2H_2O$ (M = Co, Fe, Cr).[18] These salts show good solubility in various organic solvents and high crystallinity, as well as promise in, e.g., optical resolution of cations.[18]

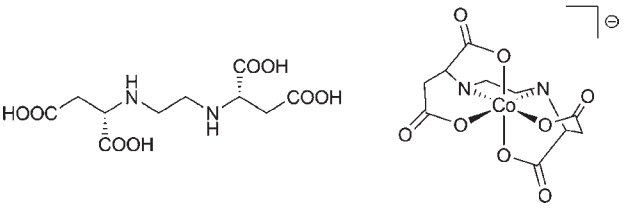

Figure 1. The structure of *S,S*-H_4EDDS and a typical anionic M(III) EDDS complex.

In this contribution, we describe the use of three of these compounds in combination with TTF and TSF in the electrosynthesis of chiral semiconducting phases in which the donor species—under the influence of the optically pure anion—form chiral undulating stacks.

RESULTS AND DISCUSSION

Synthesis of Charge Transfer Salts. All of the compounds in this work were obtained by electrocrystallization. Donor molecules (TTF and TSF) and $PPh_4[M^{III}(S,S\text{-EDDS})] \cdot 2H_2O$ (M = Co, Fe, Cr) were synthesized according to published procedures.[18−20]

Received: December 17, 2010
Published: April 04, 2011

Using H-shaped cells, the solid neutral donor molecule was placed in the anode side, and the remainder of the cell was filled with a solution of the appropriate complex, which acted as the electrolyte. Several different solvents and solvent mixtures were tested initially; it was found however that an acetonitrile/water (20:1) mixture produced crystalline materials of the highest quality. This is in agreement with our previous observations for EDDS complexes in which the presence of a small amount of water aids the crystallization of salts with lipophilic anions due to the formation of extensive H-bonding networks.[18] The electrocrystallization cells were kept at ambient temperature under constant current conditions (1 μA). The resulting salts, $(TTF)_3[Co^{III}(S,S\text{-EDDS})]_2\cdot 6H_2O$ (**1**), $(TTF)_3[Fe^{III}(S,S\text{-EDDS})]_2\cdot 5H_2O$ (**2**), $(TTF)_3[Cr^{III}(S,S\text{-EDDS})]_2\cdot 4.5H_2O$ (**3**), $(TSF)_3[Co^{III}(S,S\text{-EDDS})]_2\cdot 6H_2O$ (**4**), $(TSF)_3[Fe^{III}(S,S\text{-EDDS})]_2\cdot 6H_2O$ (**5**), and $(TSF)_3[Cr^{III}(S,S\text{-EDDS})]_2\cdot 6H_2O$ (**6**), were harvested after a period of two to three weeks and were characterized by single crystal X-ray diffraction, IR, microanalysis (where possible), and single crystal conductivity measurements.

Single Crystal X-Ray Structures. *$(TTF)_3[Co^{III}(S,S\text{-EDDS})]_2\cdot 6H_2O$ (**1**).* To varying extents, all of the investigated crystals of this compound were found to be nonmerohedrally twinned. However, solution and refinement of the crystal structure was possible using twin refinement. Compound **1** crystallizes in a chiral monoclinic space group $P2_1$ with two complex anions, three TTF units, and six molecules of water in the asymmetric unit cell (Figure 2). Hydrogen atoms of the water molecules could not be located, most likely due to the formation of a disordered H-bonding network; they were however included for formula completeness. Details of the crystal solution and refinement can be found in Table 1.

The three TTF molecules are not crystallographically identical, with one of the molecules exhibiting a significant deviation from planar geometry; the angle between the mean planes of each of the rings is 9.47°. Distances between the planes of the TTF units in the π stacks range from 3.2 to 3.7 Å. The molecules in the stack are parallel, with the angles between mean planes of the molecules below 2.3°.

To the first approximation the extended packing of the compound is typical of these types of compounds, with the TTF stacks running between columns of the complex anions, in this case along the [100] direction (Figure 3a). These stacks and columns form layers along the [110] direction, as shown in Figure 3b. There are several short contacts between the sulfur atoms of the TTF stack and carbonyl atoms of the chiral anion. This is accompanied by an elliptical helix arrangement in the stacks as described below.

Inabe has reported a mellitate salt $[TTF^+]_2[C_6(CO_2)_6H_4^{2-}]$ in which the TTF units in the stacks are mutually rotated about a central axis so as to form a helicoid-like (staircase) arrangement (Figure 4a).[11] As far as we are aware, this compound is an insulator, and certainly this would be our expectation given the misalignment of S atom orbitals in the TTF stack.

The undulation present in the cationic stacks in **1** is depicted in Figure 4b. The TTF units are laterally displaced with respect to one another—keeping their long axes parallel—such that the trace of their centroids forms a left-handed elliptical helix. This is further depicted in Figure 4c where the centroids of adjacent TTF units are linked with red lines. The period of this helical undulation is equal to the unit cell length (10.6 Å), and the elliptical amplitudes are 0.9 and 1.2 Å. Since undulations are a common feature of TTF and related stacks, it is almost certain that this motif appears in other structures, although in achiral systems both mirror images would be present.

Analysis of the average C−S bond lengths of the TTF units in the structure shows significant differences between the three independent units in the asymmetric cell. It has been demonstrated that the average bond distances in the TTF molecule and its charge follow a simple linear codependency,[21] and this allows us to assign partial charges of between +0.2 and +1.1 for the TTF units, as

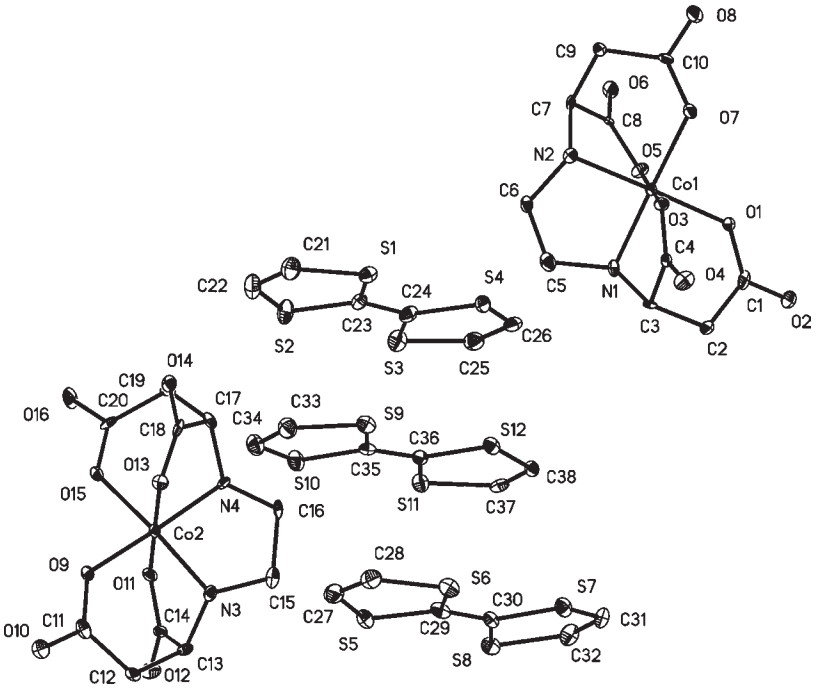

Figure 2. Solid state structure of $(TTF)_3[Co^{III}(S,S\text{-EDDS})]_2\cdot 6H_2O$ (**1**) with thermal parameters drawn at 50% probability. Water molecules and hydrogen atoms removed for clarity.

dx.doi.org/10.1021/ic102522k |*Inorg. Chem.* 2011, 50, 4039–4046

Table 1. Details of the Crystal Solutions and Refinement

compound	$(TTF)_3[Co(S,S\text{-}EDDS)]_2\cdot 6H_2O$ (**1**)	$(TTF)_3[Fe(S,S\text{-}EDDS)]_2\cdot 5H_2O$ (**2**)	$(TTF)_3[Cr(S,S\text{-}EDDS)]_2\cdot 4.5H_2O$ (**3**)[a]	$(TSF)_3[Co(S,S\text{-}EDDS)]_2\cdot 6H_2O$ (**4**)	$(TSF)_3[Fe(S,S\text{-}EDDS)]_2\cdot 6H_2O$ (**5**)	$(TSF)_3[Cr(S,S\text{-}EDDS)]_2\cdot 6H_2O$ (**6**)
formula	$C_{38}H_{48}Co_2N_4O_{22}S_{12}$	$C_{38}H_{46}Fe_2N_4O_{21}S_{12}$	$C_{40}H_{74}Cr_4N_8O_{45}$	$C_{38}H_{48}Co_2N_4O_{22}Se_{12}$	$C_{38}H_{48}Fe_2N_4O_{22}Se_{12}$	$C_{38}H_{48}Cr_2N_4O_{22}Se_{12}$
fw	1415.38	1391.21	1595.07	1978.18	1972.02	1964.32
cryst size	0.24 × 0.10 × 0.02	0.24 × 0.08 × 0.08	0.18 × 0.18 × 0.07	0.20 × 0.17 × 0.14	0.30 × 0.04 × 0.03	0.17 × 0.08 × 0.01
cryst syst	monoclinic	triclinic	monoclinic	monoclinic	monoclinic	monoclinic
space group	$P2_1$	$P1$	$P2_1$	$P2_1$	$P2_1$	$P2_1$
Z	2	2	2	2	2	2
a (Å)	10.5591(2)	10.4392(2)	16.4999(8)	10.3219(5)	10.9413(5)	10.8846(5)
b (Å)	10.3507(2)	10.5270(2)	10.7581(4)	24.9435(11)	10.4374(4)	10.3773(5)
c (Å)	24.2916(5)	23.9133(3)	18.9837(9)	10.7594(5)	25.0015(11)	25.0263(10)
α (deg)	90	90	90	90	90	90
β (deg)	93.3972(19)	90	102.388(2)	90.399(3)	94.188(2)	94.094(3)
γ (deg)	90	90	90	90	90	90
V (Å^3)	2650.26(9)	2627.92(8)	3291.3(3)	2770.1(2)	2847.5(2)	2819.6(2)
d_{calcd} (mg/cm^3)	1.774	1.758	1.610	2.372	2.300	2.314
temp (K)	100(2)	100(2)	120(2)	120(2)	120(2)	120(2)
radiation (Å)	Mo Kα (λ = 0.71073)	Mo Kα (λ = 0.71073)	Mo Kα (λ = 0.71073)	Mo Kα (λ = 0.71073)	Mo Kα (λ = 0.71073)	Mo Kα (λ = 0.71073)
2θ max	32.61	27.49	27.50	27.50	27.49	27.48
μ (mm^{-1})	1.182	1.110	0.756	8.563	8.257	8.210
Flack parameter	0.001(11)	0.010(16)	0.03(2)	0.05(3)	0.074(14)	0.206(19)
F_{000}	1452	1428	1652	1884.0	1880	1872
total no. of reflections	35590	39836	42041	55875	41116	28563
no. of independent reflections	35590	39836	15069	12654	41116	28563
R_{int}	b	b	0.1025	0.1095	b	b
R1, [$I > 2\sigma(I)$]	0.0511	0.0394	0.0778	0.0731	0.0876	0.0950
wR2	0.1158	0.0910	0.1767	0.1648	0.1619	0.1884
GoF	0.984	0.991	1.039	1.040	1.043	1.081

[a] Only the anionic sublattice of this compound was refined; the quoted values therefore, including the formula, relate only to this sublattice. [b] R_{int} values for the twinned structures were not given, as the solution and refinement were performed using nonmerged data.

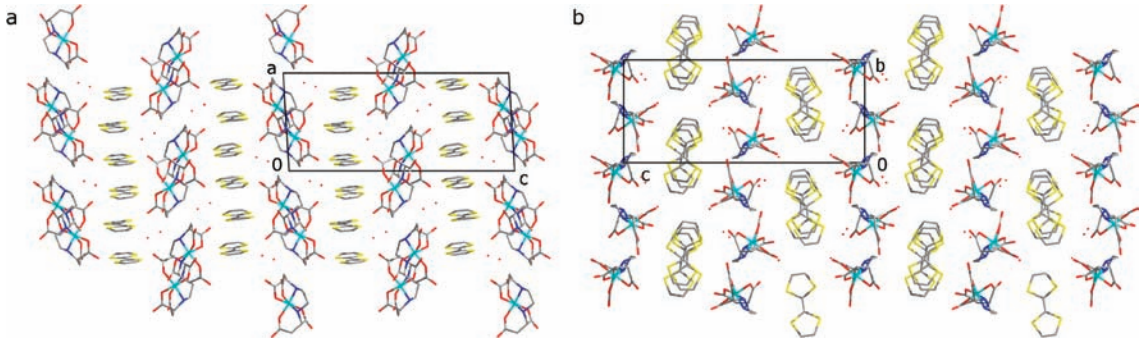

Figure 3. Solid state packing of $(TTF)_3[Co^{III}(S,S\text{-}EDDS)]_2\cdot 6H_2O$ (**1**), (a) view from [010] and (b) [100] directions.

shown in Figure 5. This charge localization results most likely from the different interactions between each of the TTF molecules and the chiral anions and/or asymmetric stacking behavior. As a result, the compound exhibits relatively low conductivity (*vide infra*).

*$(TTF)_3[Fe^{III}(S,S\text{-}EDDS)]_2\cdot 5H_2O$ (**2**).* Similar to its cobalt(III) analogue, all of the examined crystals of this compound were nonmerohedrally twinned; the twin components were identified using Platon TwinRotMat.[22] The structure (Figure 6) was solved in a triclinic $P1$ unit cell and was refined using SHELX twin refinement.[23] Due to a large amount of disorder in the structure, further reduction of symmetry was not possible. Attempts to solve the structure in the apparent

dx.doi.org/10.1021/ic102522k |*Inorg. Chem.* 2011, 50, 4039–4046

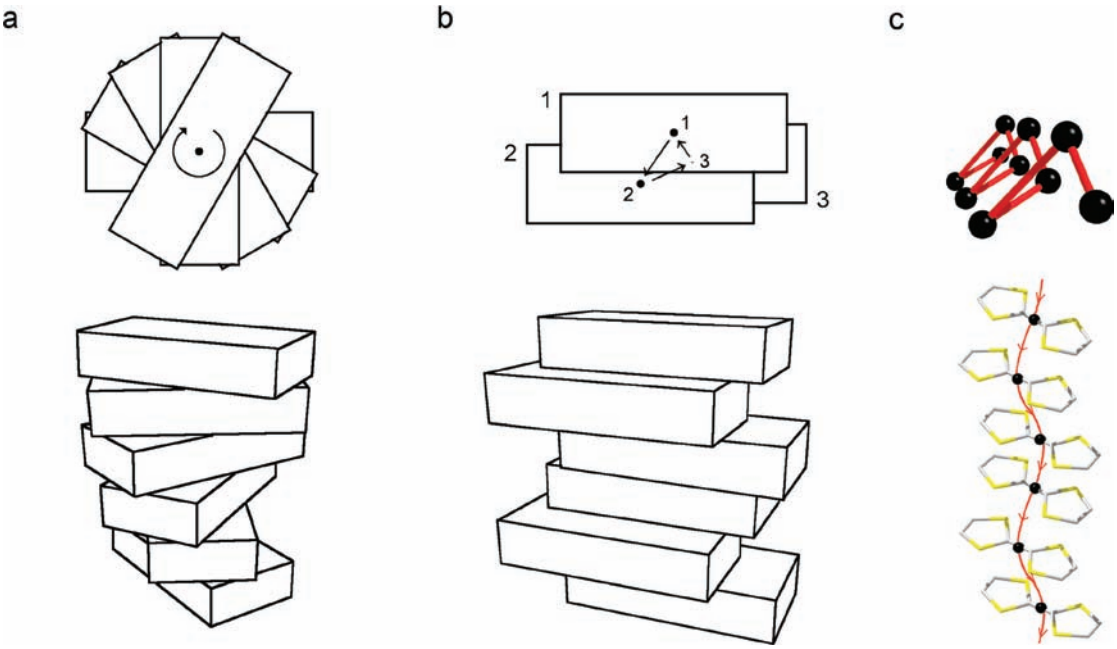

Figure 4. Top and side views of helical motifs: (a) Inabe's $[TTF^{+}]_2[C_6(CO_2)_6H_4^{2-}]$ in which the TTF units—here shown as blocks—are mutually rotated about the main axis so as to form a staircase-like helix. (b) $(TTF)_3[Co^{III}(S,S\text{-EDDS})]_2\cdot 6H_2O$ (**1**) in which the TTF units are laterally translated such that the centroids trace a left-handed elliptical helix. (c) Plots from the X-ray structure of **1** with red lines linking the centroids (black spheres) of adjacent TTF units.

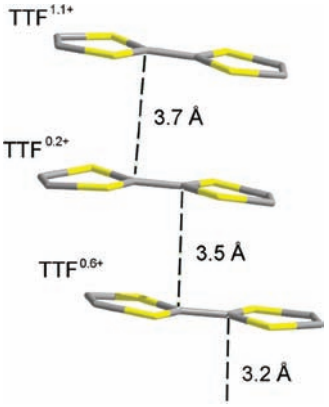

Figure 5. Average distances between the planes of the TTF molecules in the stacks and the charges calculated from bond length analysis.

orthorhombic unit cell did not result in a satisfactory solution.

The asymmetric part of the cell contains four complex anions, 10 molecules of water, and two stacks of three TTF molecules each, with the TTF molecules disordered between two positions with an occupation factor of a half. No hydrogen atoms for the water molecules were located. Details of the structure solution and refinement are summarized in Table 1.

The extended packing in the solid state is analogous to that of the cobalt(III) compound. Calculation of the exact charges on each of the TTF units is precluded due to the disorder in the structure.

*$(TTF)_3[Cr^{III}(S,S\text{-EDDS})]_2\cdot 4.5H_2O$ (**3**).* Solution of the single crystal diffraction data collected for this compound was possible for only the anionic sublattice of the assembly. This suggests that the compound might have an incommensurate structure, relatively common for this type of compound.[10,24,25] Unfortunately, the structure of the cationic part of the assembly was not obtained. The presence of the organic donor cationic sublattice is however demonstrated by the elemental microanalysis, IR spectrum (presence of peaks characteristic for oxidized TTF),[26] and the results of the conductivity measurements (*vide infra*). Furthermore, all of the obtained crystals were dark brown/black, a color characteristic of TTF charge transfer compounds.

The anionic sublattice crystallizes in the monoclinic $P2_1$ space group. The asymmetric part of the unit cell contains four complex anions and nine water molecules (Figure 7). One of the complex anions and the water molecules were modeled as disordered. The organic backbone of the anion in question was modeled as disordered between two alternative positions, with occupation factors of a half. As a result of the disorder, the thermal ellipsoids in this anion are significantly larger compared to the remaining ions. The effect is especially apparent in the carbonyl groups of the compound. Details of the crystal solution and refinement can be found in Table 1.

Due to lack of structure of the cationic moieties, the exact stoichiometry of the compound was not established. It is however expected to be similar to the cobalt(III) and iron(III) analogues, considering the similarities of the IR spectra and electrical conductivity of all three compounds. The proposed formula, as supported by elemental analysis, is therefore $(TTF)_3[Cr^{III}(S,S\text{-EDDS})]_2\cdot 4.5H_2O$.

*$(TSF)_3[M^{III}(S,S\text{-EDDS})]_2\cdot 6H_2O$ (**4**, **5**, and **6**).* All of the obtained TSF salts were found to have very similar solid state structures, analogous to that of $(TTF)_3[Co^{III}(S,S\text{-EDDS})]_2\cdot 6H_2O$ (**4**). The compounds crystallize in a monoclinic $P2_1$ space group. The asymmetric units comprise three TSF molecules, two complex anions, and six water molecules (Figure 8). As with the previous structures, the hydrogen atoms of the water molecules were not located.

dx.doi.org/10.1021/ic102522k |*Inorg. Chem.* 2011, 50, 4039–4046

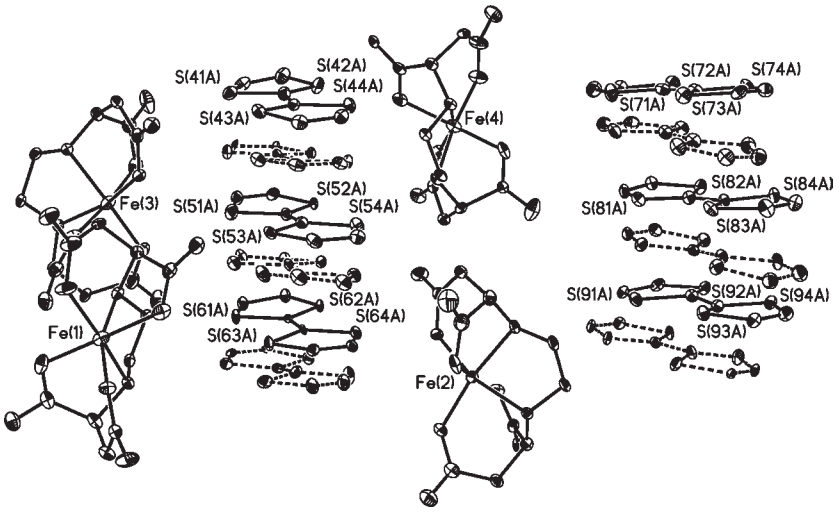

Figure 6. Solid state structure of $(TTF)_3[Fe^{III}(S,S\text{-EDDS})]_2 \cdot 5H_2O$ (**2**) with thermal parameters drawn at 50% probability. Water molecules and hydrogen atoms were removed for clarity.

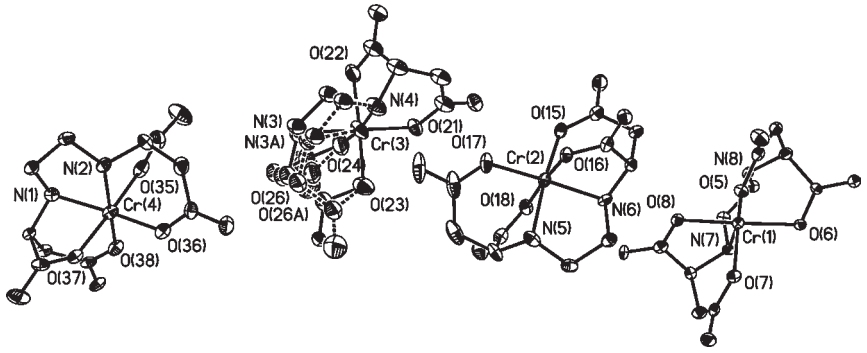

Figure 7. Solid state structure of the anionic sublattice of $(TTF)_3[Cr^{III}(S,S\text{-EDDS})]_2 \cdot 4.5H_2O$ (**3**). Hydrogen atoms and solvent molecules were removed for clarity.

The extended packing of the compound is directly comparable with that of $(TTF)_3[Co^{III}(S,S\text{-EDDS})]_2 \cdot 6H_2O$ (**1**). The TSF stacks form layers which alternate with layers of the complex anions. The stacks also undulate in a similar manner to those in **1** (Figure 4b,c) with a period of 10.8 Å and elliptical amplitudes 0.7 and 1.4 Å.

The average Se−C bond lengths within each of the TSF molecules vary between 1.86 and 1.91 Å. This suggests that, as with the TTF salts, charge localization occurs, and each of the TSF units has a different oxidation state, although there is not yet a published analysis that allows us to define this further.

Conductivity Measurements. Conductivity measurements of all of the obtained compounds were made at ambient and variable temperatures using either a two or four probe DC setup, depending on the crystal size and geometry.

*$(TTF)_3[M^{III}(S,S\text{-EDDS})]_2 \cdot xH_2O$ (**1**, **2**, and **3**).* All of the TTF salts exhibit relatively low, and similar, average ambient temperature conductivities: $\sigma_{RT}{}^{\mathbf{1}} = 1.1 \times 10^{-5}$ S·cm^{-1}, $\sigma_{RT}{}^{\mathbf{2}} = 1.3 \times 10^{-5}$ S·cm^{-1}, $\sigma_{RT}{}^{\mathbf{3}} = 6.9 \times 10^{-6}$ S·cm^{-1}.

The temperature dependence of the conductivity for all of the compounds follows an exponential curve, typical for semiconductive materials. $(TTF)_3[Co^{III}(S,S\text{-EDDS})]_2 \cdot 6H_2O$ additionally exhibits a small repeatable and reversible step-change in conductivity at 260 K, which is likely due to a structural change at that temperature. High temperature crystallographic data would help us to address this behavior, but the twinning and disorder in the crystals makes this impractical. The graphs of the temperature dependence of the conductivity for **1**, **2**, and **3** can be found in the Supporting Information.

The temperature dependence of the electrical conductivity in these materials follows the Arrhenius law. The dependence of the natural logarithm of conductivity $[\ln(\sigma)]$ on the inverse of the temperature $(1/T)$ therefore allows for the calculation of the activation energy (E_a; Figure 9). The calculated values are $E_a{}^{\mathbf{1}} = 0.244$ eV, $E_a{}^{\mathbf{2}} = 0.357$ eV, and $E_a{}^{\mathbf{3}} = 0.252$ eV, which are in the range typical for TTF materials. It is worth noticing that the value calculated for the iron(III) analogue is significantly higher than those obtained for the cobalt(III) and chromium(III) compounds.

*$TSF_3[M^{III}(S,S\text{-EDDS})]_2 \cdot 6H_2O$ (**4**, **5**, and **6**).* The ambient temperature conductivities (σ_{RT}) of the TSF materials **4**−**6** were 5.7×10^{-4} S·cm^{-1}, 2.8×10^{-5} S·cm^{-1}, and 2.8×10^{-4} S·cm^{-1}. As might be expected, these are between 1 and 2 orders of magnitude higher than their TTF analogues (*vide supra*).

As with their TTF analogues, all of the TSF salts exhibit semiconducting behavior upon cooling. Additionally, small reversible changes of conductivity, again most likely due to structural changes, were observed for $(TSF)_3[Co^{III}(S,S\text{-EDDS})]_2 \cdot 6H_2O$ (**4**) and $(TSF)_3[Cr^{III}(S,S\text{-EDDS})]_2 \cdot 6H_2O$ (**6**). Activation energies for all of the compounds, before and after the phase changes, were

dx.doi.org/10.1021/ic102522k |*Inorg. Chem.* 2011, 50, 4039–4046

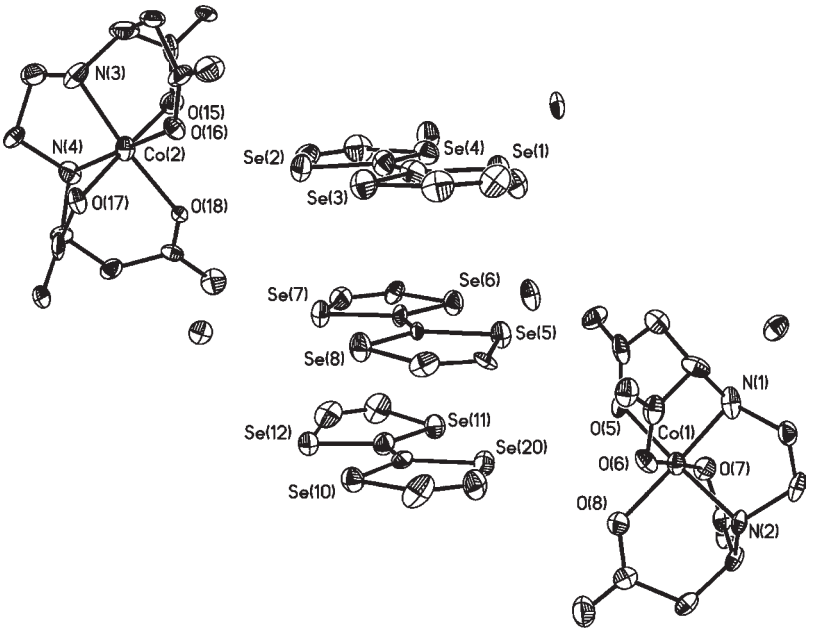

Figure 8. Solid state structure of the anionic sublattice of $(TSF)_3[Co^{III}(S,S\text{-EDDS})]_2 \cdot 6H_2O$ (**4**). Hydrogen atoms were removed for clarity. Compounds **4**−**6** are isostructural.

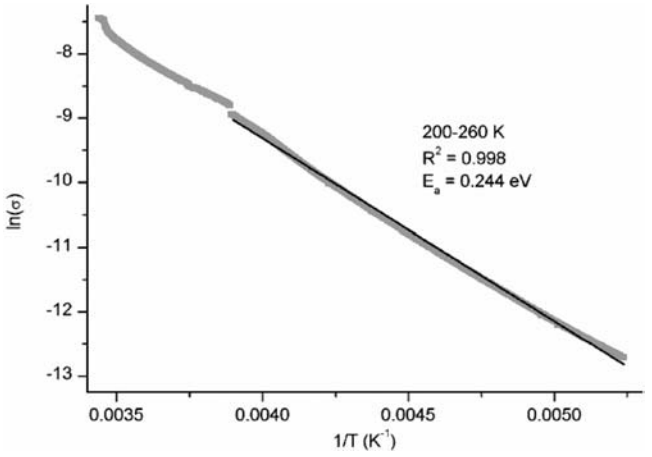

Figure 9. Dependence of natural logarithm of conductivity of **1** on reciprocal temperature and the linear fit of the data.

Table 2. The Calculated Activation Energies of $(TSF)_3[M^{III}(S,S\text{-EDDS})]_2 \cdot 6H_2O$ (M = Co, Fe, Cr)

compound	temperature range (K)	E_a (eV)
$(TSF)_3[Co^{III}(S,S\text{-EDDS})]_2 \cdot 6H_2O$ (4)	200−250	0.106
	170−200	0.135
$(TSF)_3[Fe^{III}(S,S\text{-EDDS})]_2 \cdot 6H_2O$ (5)	210−300	0.200
$(TSF)_3[Cr^{III}(S,S\text{-EDDS})]_2 \cdot 6H_2O$ (6)	250−285	0.107
	190−250	0.125
	125−150	0.093

calculated, and the results are summarized in Table 2. The calculated values are much lower than those obtained for the TTF analogues, which is expected due to broader band formation originating with Se as opposed to S orbitals. It is worth noting that the activation energy obtained for the iron(III) analogue is significantly higher than those obtained for the other compounds, as was observed for the TTF salts. We do not believe this effect to be caused by the change of the size of the complex anion, as the average bond lengths to the metal centers change in Co < Fe ≤ Cr order.

DFT Calculations. In order to investigate the relatively low conductivity of the TTF based compounds, simple DFT calculations using the solid state structure of $(TTF)_3[Co^{III}(S,S\text{-EDDS})]_2 \cdot 6H_2O$ were performed. The calculation only considers 1-dimensional conduction along the chain of TTF molecules considering the three independent TTF moieties in the unit cell and assumes that the highest occupied and the lowest unoccupied bands can be expressed as a linear combination of the TTF HOMO and LUMO orbitals. The one-dimensional band structure is determined by the electronic coupling (V) between the HOMO and LUMO orbitals, which is more rigorously defined as the integral $\langle \phi_i | F | \phi_j \rangle$ where ϕ_i and ϕ_j are the orbitals and F is the Fock operator. The calculation was performed using the ZINDO and B3LYP/6-31G* methods.[27−29]

From the interorbital couplings given in Table 3, it is apparent that two different types of TTF molecules are present in the structure. Two of the TTF molecules are of the same type (A in Figure 10), whereas the third one is significantly different (B). This is consistent with the findings from the solid state structure, suggesting that the charge on one of the TTF molecules is close to zero (molecule B). It is worth noting that while the two charged molecules (molecules A) are quite similar, they are not equivalent. As a result of these differences, the coupling between molecule types A and B is significantly smaller than coupling between two molecules of type A.

In order to additionally explain the conductive properties of the compound, a one-dimensional band structure along the largest coupling direction was computed. For the purposes of this calculation, the unit cell is the AAB unit of TTF molecules (the counterions and solvent molecules were discarded). The single

dx.doi.org/10.1021/ic102522k |*Inorg. Chem.* 2011, 50, 4039–4046

Table 3. Absolute Coupling Values in cm^{-1}[a]

	ZINDO		B3LYP/6-31G*	
coupling	HOMO−HOMO	LUMO−LUMO	HOMO−HOMO	LUMO−LUMO
aa	4314.2	869.9	5874.8	1850.2
ab	1568.6	292.5	2440.8	368.5
ab′	1912.0	588.9	4110.1	912.1

[a] See Figure 10 for the coupling directions.

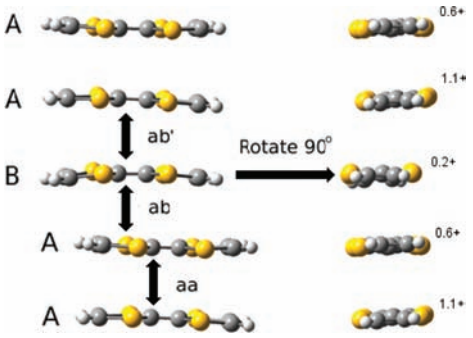

Figure 10. Inequivalent couplings in the $(TTF)_3[Co^{III}(S,S\text{-EDDS})]_2 \cdot 6H_2O$ (**1**) structure. Charges calculated from the crystal structure.

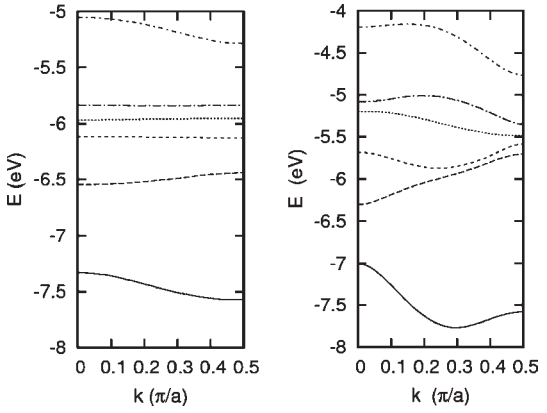

Figure 11. Band structure diagrams for (left) the "AAB" unit and (right) the hypothetical "AAA" unit. The bands shown are valence−2 to conduction+2. The valence band (third band from the bottom) is 2/3 filled (due to the charge stoichiometry of the crystal). Computed at B3LYP/6-31G* level of theory.

dimension of the band is the axis through the TTF molecules. For comparison, the band structure for the hypothetical AAA unit was also calculated.

Interestingly, in the "AAB" case, the valence band is very flat (Figure 11, left). The negligible band dispersion along the TTF is indicative of orbital localization within the unit cell, and it is therefore consistent with the crystallographic results. Consequently, the material behaves as a semiconductor (the gap between the valence and conduction band is calculated to be 0.15 eV at the smallest separation), which compares reasonably well with the activation energy (half the band gap) calculated from the Arrhenius plot (*vide supra*). However, in the hypothetical "AAA" case, the valence band is considerably more dispersed (the difference between minimum and maximum values is 0.29 eV), and since this band would be only partially occupied, this hypothetical system would be expected to behave as a metal.

CONCLUSIONS

Rikken's original observation of MCA in a twisted bismuth wire inspired us and other groups[7−11] to explore the possibility of creating chiral conductors from optically pure molecular components. This is partly achieved here, but the conductivity is not yet high enough for MCA measurements as a result of charge localization in the TTF/TSF stacks. The helical undulations depicted in Figure 4 are at least partly responsible for this localization, although of course the disruption is rather less profound than in Inabe's twisted helix compound.[11] Coronado and coworkers have recently reported a structure based on an optically pure ET derivative,[10] which despite the inherent chirality has a highly symmetrical arrangement of the charge-carrying motif. The material is a metallic conductor (65 $S \cdot cm^{-1}$) as well as a ferromagnet, but no magnetochiral anisotropy was observed. On the basis of these observations, we propose that it may be fruitful to consider optically pure anion systems which are expected to have a more moderate influence on the asymmetry of the cation stacks than that which we see in the phases reported here.

EXPERIMENTAL SECTION

General Considerations. *S,S*-EDDS was obtained from Innospec Inc. and used without further purification. All other solvents and chemicals were purchased from Sigma-Aldrich, Acros, or Alfa Aesar and used without further purification. TTF, TSF, and $PPh_4[M^{III}(S,S\text{-EDDS})] \cdot 2H_2O$ were prepared according to the literature procedures.[18−20] Electrocrystallizations were performed in custom-made glass H-tubes with anode and cathode compartments separated by a glass frit. The cells were prepared under a dinitrogen atmosphere in a drybox using dry solvents and sealed using a rubber septum (Suba Seal). Electrodes were made of platinum wire (Ø = 1 mm, Goodfellow Cambridge Ltd.). Infrared spectra were measured using a Perkin-Elmer FTIR spectrometer. The crystal data were collected using an Oxford Diffraction Gemini R and Siemens SMART CCD single crystal diffractometers using a Mo Kα (λ = 0.7073 Å) radiation source. Structures were solved using direct methods: SHELX (TREF)[23,30] with additional light atoms found by Fourier methods. Crystal refinement was performed using SHELX97.[23] Publication data were prepared using SHELXTL and WINGX.[31] Electrical conductivity measurements were performed with a Keithley 2001 Multimeter using typical two and four probe setups. Contacts to the crystal were made by gold wires (25 μm, Goodfellow Cambridge Ltd.) and attached with carbon cement (Agar Scientific).

Electrocrystallization—General Procedure. The tetraphenylphosphonium salt of the chiral counterion (25 mg) was dissolved in dry MeCN (20 mL) under dinitrogen in a drybox. The appropriate donor (TTF 5 mg, TSF 8 mg) was placed in the anode chamber of the electrocrystallization cell in the solid form. The cell was then carefully filled with the solution of the counterion, fitted with platinum electrodes, and sealed. The cell was then removed from the drybox, and water (1 mL) was injected into the sealed cell. A constant current of 1 μA was applied across each cell, and after two to four weeks, dark crystals were harvested from the anode.

$(TTF)_3[Co^{III}(S,S\text{-EDDS})]_2 \cdot 6H_2O$. IR ($cm^{-1}$): ν 3198, 1655, 1438, 1396, 1339, 1283, 1213, 1199, 1113, 1091, 1044, 1017, 871, 731, 700.

$(TTF)_3[Fe^{III}(S,S\text{-EDDS})]_2 \cdot 5H_2O$. IR ($cm^{-1}$): ν 3188, 1603, 1439, 1350, 1314, 1272, 1207, 1100, 1045, 1020, 974, 912, 875, 807, 788, 656.

dx.doi.org/10.1021/ic102522k |*Inorg. Chem.* 2011, 50, 4039–4046

(TTF)$_3$[Cr^{III}(S,S-EDDS)]$_2$·4.5H$_2$O. IR (cm^{-1}): *ν* 3580, 3176, 3048, 2917, 1661, 1629, 1592, 1472, 1445, 1392, 1366, 1348, 1326, 1256, 1221, 1205, 1094, 1050, 1019, 1003, 914, 869, 813, 800, 724, 699, 678

Elemental analysis found (calculated for $C_{38}H_{45}N_4O_{20.5}S_{12}Cr_2$), %: C, 33.16 (33.20); H, 3.38 (3.30); N, 4.45 (4.08).

(TSF)$_3$[Co^{III}(S,S-EDDS)]$_2$·6H$_2$O. IR (cm^{-1}): *ν* 3189, 3032, 1655, 1619, 1596, 1571, 1455, 1376, 1342, 1275, 1236, 1214, 1199, 1078, 1058, 1043, 1017, 918, 874, 667.

Elemental analysis found (calculated for $C_{38}H_{48}N_4O_{22}Se_{12}Co_2$), %: C, 23.22 (23.07); H, 2.53 (2.45); N, 2.80 (2.83).

(TSF)$_3$[Fe^{III}(S,S-EDDS)]$_2$·6H$_2$O. IR (cm^{-1}): *ν* 3209, 3031, 2931, 1592, 1447, 1355, 1311, 1232, 1204, 1101, 1058, 1018, 973, 956, 910, 864, 812, 713.

Elemental analysis found (calculated for $C_{38}H_{48}N_4O_{22}Se_{12}Fe_2$), %: C, 22.82 (23.14); H, 2.66 (2.45); N, 2.90 (2.84).

(TSF)$_3$[Cr^{III}(S,S-EDDS)]$_2$·6H$_2$O. IR (cm^{-1}): *ν* 3575, 3174, 2917, 1660, 1624, 1588, 1444, 1389, 1372, 1315, 1270, 1216, 1201, 1098, 1078, 1047, 994, 946, 913, 865, 806, 720, 699.

Elemental analysis found (calculated for $C_{38}H_{48}N_4O_{22}Se_{12}Cr_2$), %: C, 23.66 (23.24); H, 2.58 (2.46); N, 2.96 (2.85).

■ ASSOCIATED CONTENT

Ⓢ Supporting Information. Graphs of temperature dependence of conductivity and Arrhenius plots for compounds **2**−**6**. This material is available free of charge via the Internet at http://pubs.acs.org.

■ AUTHOR INFORMATION

Corresponding Author
*E-mail: peter.scott@warwick.ac.uk.

■ ACKNOWLEDGMENT

We thank the EPSRC for funding and the EPSRC National Crystallography Service and Oxford diffraction for collecting the crystal data. The Oxford Diffraction Gemini XRD system was obtained through the Science City Advanced Materials project: Creating and Characterising Next Generation Advanced Materials, with support from Advantage West Midlands (AWM) and part funded by the European Regional Development Fund (ERDF). We thank James Barker and Innospec Inc. for a sample of *S,S*-EDDS.

■ REFERENCES

(1) Rikken, G. L. J. A.; Folling, J.; Wyder, P. *Phys. Rev. Lett.* **2001**, *87* (23), 236602.
(2) Krstic, V.; Rikken, G. L. J. A. *Chem. Phys. Lett.* **2002**, *364* (1−2), 51–56.
(3) Coronado, E.; Galan-Mascaros, J. R. *J. Mater. Chem.* **2005**, *15* (1), 66–74.
(4) Krstic, V.; Roth, S.; Burghard, M.; Kern, K.; Rikken, G. L. J. A. *J. Chem. Phys.* **2002**, *117* (24), 11315–11319.
(5) Gomar-Nadal, E.; Veciana, J.; Rovira, C.; Amabilino, D. *Adv. Mater.* **2005**, *17* (17), 2095–2098.
(6) Yamamoto, T.; Fukushima, T.; Kosaka, A.; Jin, W.; Yamamoto, Y.; Ishii, N.; Aida, T. *Angew. Chem., Int. Ed.* **2008**, *47* (9), 1672–1675.
(7) Martin, L.; Day, P.; Horton, P.; Nakatsuji, S.; Yamada, J.; Akutsu, H. *J. Mater. Chem.* **2010**, *20* (14), 2738–2742.
(8) Brezgunova, M.; Shin, K.-S.; Auban-Senzier, P.; Jeannin, O.; Fourmigue, M. *Chem. Commun.* **2010**, *46* (22), 3926–3928.
(9) Coronado, E.; Curreli, S.; Giménez-Saiz, C.; Gómez-García, C. J.; Roth, J. *Synth. Met.* **2005**, *154* (1−3), 241–244.
(10) Galán-Mascarós, J. R.; Coronado, E.; Goddard, P. A.; Singleton, J.; Coldea, A. I.; Wallis, J. D.; Coles, S. J.; Alberola, A. *J. Am. Chem. Soc.* **2010**, *132* (27), 9271–9273.
(11) Inabe, T. *J. Mater. Chem.* **2005**, *15* (13), 1317–1328.
(12) Avarvari, N.; Wallis, J. D. *J. Mater. Chem.* **2009**, *19* (24), 4061–4076.
(13) Wallis, J. D.; Karrer, A.; Dunitz, J. D. *Helv. Chim. Acta* **1986**, *69* (1), 69–70.
(14) Zambounis, J. S.; Mayer, C. W.; Hauenstein, K.; Hilti, B.; Hofherr, W.; Pfeiffer, J.; Buerkle, M.; Rihs, G. *Mater. Res. Soc. Symp. Proc.* **1992**, *247*, 509–13.
(15) Coronado, E.; Galan-Mascaros, J. R.; Gomez-Garcia, C. J.; Murcia-Martinez, A.; Canadell, E. *Inorg. Chem.* **2004**, *43*, 8072–8077.
(16) Chmel, N. P.; Allan, L. E.; Becker, J. M.; Clarkson, G. J.; Turner, S. S.; Scott, P. *Dalton Trans.* **2011**, *40*, 1722–1731.
(17) Neal, J. A.; Rose, N. J. *Inorg. Chem.* **1968**, *7* (11), 2405–2412.
(18) Chmel, N. P.; Howson, S. E.; Allan, L. E. N.; Barker, J.; Clarkson, G. J.; Turner, S. S.; Scott, P. *Dalton Trans.* **2010**, *39* (11), 2919–2927.
(19) Melby, L. R.; Hartzler, H. D.; Sheppard, W. A. *J. Org. Chem.* **1974**, *39* (16), 2456–2458.
(20) Takimiya, K.; Jeon, H. J.; Otsubo, T. *Synthesis* **2005**, *2005* (16), 2810–2813.
(21) Clemente, D. A.; Marzotto, A. *J. Mater. Chem.* **1996**, *6* (6), 941–946.
(22) Spek, A. *J. Appl. Crystallogr.* **2003**, *36* (1), 7–13.
(23) Sheldrick, G. M. *Acta Crystallogr., Sect. A* **2008**, *64*, 112–122.
(24) Makovicky, E.; Hyde, B. In *Inorganic Chemistry*; Springer: Berlin, 1981; Vol. 46, pp 101−170.
(25) Coronado, E.; Galán-Mascarós, J. R.; Gómez-García, C. J.; Martínez-Ferrero, E.; van Smaalen, S. *Inorg. Chem.* **2004**, *43* (16), 4808–4810.
(26) Matsuzaki, S.; Koga, N.; Moriyama, I.; Toyoda, K. *Bull. Chem. Soc. Jpn.* **1983**, *56* (7), 2090–2092.
(27) Bacon, A. D.; Zerner, M. C. *Theor. Chim. Acta* **1979**, *53* (1), 21–54.
(28) Becke, A. D. *J. Chem. Phys.* **1993**, *98* (7), 5648–5652.
(29) Lee, C.; Yang, W.; Parr, R. G. *Phys. Rev. B* **1988**, *37* (2), 785.
(30) Sheldrick, G. M. *Acta Crystallogr., Sect. A* **1990**, *46*, 467–473.
(31) Farrugia, L. *J. Appl. Crystallogr.* **1999**, *32* (4), 837–838.